

# A Visual Analytics Approach to Monitor Time-Series Data with Incremental and Progressive Functional Data Analysis

Shilpika\*

University of California, Davis

Takanori Fujiwara\*

University of California, Davis

Naohisa Sakamoto<sup>†</sup>

Kobe University

Jorji Nonaka<sup>‡</sup>

RIKEN R-CCS

Kwan-Liu Ma\*

University of California, Davis

## ABSTRACT

Many real-world applications involve analyzing time-dependent phenomena, which are intrinsically functional—consisting of curves varying over a continuum, which is time in this case. When analyzing continuous data, functional data analysis (FDA) provides substantial benefits, such as the ability to study the derivatives and to restrict the ordering of data. However, continuous data inherently has infinite dimensions, and FDA methods often suffer from high computational costs. This is even more critical when we have new incoming data and want to update the FDA results in real-time. In this paper, we present a visual analytics approach to consecutively monitor and review the changing time-series data with a focus on identifying outliers by using FDA. To perform such an analysis while addressing the computational problem, we introduce new incremental and progressive algorithms that promptly generate the magnitude-shape (MS) plot, which reveals both the functional magnitude and shape outlyingness of time-series data. In addition, by using an MS plot in conjunction with an FDA version of principal component analysis, we enhance the analyst’s ability to investigate the visually-identified outliers. We illustrate the effectiveness of our approach with three case studies using real-world and synthetic datasets.

**Index Terms:** Human-centered computing—Visualization—Visualization application domains—Visual analytics

## 1 INTRODUCTION

To ensure normal operation and adequate performance of hardware systems such as those in an assembly plant or a supercomputer center, various monitoring mechanisms have been introduced to collect data about all aspects of the systems at high frequency in real-time [28, 29]. The ability to instantaneously process and analyze the resulting time-series data thus becomes pertinent to examining various underlying system phenomena to detect and promptly react to system failures or inefficiency. High-velocity time-series data is intrinsically functional as it can be represented in the form of curves or surfaces with weak assumptions of smoothness being permitted [44]. Functional data analysis (FDA) is a branch of statistics for analyzing such data [32]. FDA incorporates statistical methodologies to capture the underlying properties and structure of the data. The statistical methods and models in FDA are typically presented in the form of continuous functions [31]. A wide range of methods have been developed to handle functional data, such as functional principal component analysis (FPCA), functional regression models, and functional canonical correlation analysis [31]. As these names indicate, many FDA methods resemble those developed for conventional discrete analysis. However, because FDA handles data with continuous functions, FDA has advantages in studying the derivatives of the data and maintaining the temporal order of data [44]. Recently, FDA has seen tremendous growth with applications in various fields, such as biology, meteorology, medicine, finance, and engineering [1, 25, 45]. While FDA methods provide new capabilities for analyzing time-series data, they often suffer from their

high computational costs, which increase with the number of time points. This can be a critical problem with real-world monitoring applications as they keep generating new time points, resulting in infinitely long time series.

With this work, we aim to reduce the computational overheads of using FDA on streaming time-series data while retaining the benefits of in-depth analysis capabilities provided by FDA. To do so, we introduce a visual analytics approach for continuously monitor and review time-series data that grows over time with a focus on identifying outliers by using FDA. In particular, we design new incremental and progressive algorithms that promptly generate the magnitude-shape (MS) plot [4], which reveals outlier time-series by depicting the outlyingness of both the functional magnitude and shape of multiple input time-series. These incremental and progressive updates to the previously computed results address the computational overhead introduced by handling growing time series data in bulk. In addition, with the support of FPCA, our approach help analysts investigate the visually-identified outliers from the MS plot.

Our main contributions are as follows:

- New incremental and progressive algorithms to generate the MS plot, which enables analyses of time-series data collected from online data streams.
- Augmentation of analysis using the MS plot with FPCA and interactive visualization to aid reviewing clusters identified from the MS plot.
- Three case studies with multiple real-world datasets demonstrate the effectiveness of our approach in two different settings: cases when (1) new time points and (2) new independent time-series are added, respectively.

## 2 BACKGROUND AND RELATED WORK

In this section, we first discuss relevant works in streaming data visualization and then provide a background to FDA, including functional principal component analysis (FPCA) and magnitude-shape (MS) plots [4]—FDA methods utilized in our work.

### 2.1 Streaming Data Visualization

Visualization of streaming data is a challenging task since visualizations need to be continually updated with incoming data. The major bottlenecks in visualizing continuous streams of data are computational cost and cognitive load. Within these bottlenecks, the cognitive load is discussed by Krstajic and Keim [20]. For example, they summarized the trade-offs between updating a view when a new data point is fed from the stream, which leads to loss of mental map, or not updating a view, which leads to loss of information. Dasgupta et al. [5], through their comprehensive survey, further characterized challenges in perception and cognition of streaming visualizations and methods developed to address the challenges. In this paper, while we consider the cognitive load of visualizations, we mainly address the computational cost when producing visualizations.

Some of the past works on incremental updates to visualize up-to-date results while avoiding rising computation costs. For example, Tanahashi et al. [38] built a storyline visualization for streaming data by utilizing the previous steps’ storylines when deciding the new data points’ layout. Liu et al. [22] introduced a streaming tree

\*e-mail: {fshilpika, tfujiwara, klma}@ucdavis.edu

<sup>†</sup>e-mail: naohisa.sakamoto@people.kobe-u.ac.jp

<sup>‡</sup>e-mail: jorji@riken.jp

cut algorithm to instantly detect and visualize incoming topics from text stream analysis. Crnovrsanin et al. [2] developed an incremental force-directed layout algorithm with GPU acceleration. Several works also developed and enhanced incremental methods for visual analysis of high-dimensional and time-series data, including dimensionality reduction [7, 27] and change-point detection methods [18]. Katragadda et al. [17] developed VASream, a visual analytics system that can handle high-velocity streaming data by using hardware and software sandbox environment optimized to streaming data analysis workflow.

Another potential approach for streaming data analysis is the use of progressive visual analytics [41]. Progressive visual analytics provides reasonable intermediate results within a required latency when the computational cost for an entire calculation is too high. This latency requirement is common with streaming data visualizations. Therefore, several researchers developed progressive algorithms for streaming visualization, such as the progressive version of t-SNE [30] and time-series clustering [18].

Compared with the existing works above, our work addresses the problem when using an FDA method to generate visualizations from data streams. Our algorithm demonstrates a new capability for visual analytics of functional data, including time-series data, in a streaming, timely manner.

## 2.2 Functional Data Analysis

Data procured from continuous phenomena of space and/or time and allowed to be represented in the form of smooth functions, which is called functional data. For example, sensor readings of multiple temperature measurements at different components in a supercomputer can be viewed as multiple multivariate functions  $\{\mathbf{X}_1, \dots, \mathbf{X}_N\}$  defined on  $N$  machine components.  $\mathbf{X}_n$  is a single multivariate function of the temperature at location  $n \in \{1, \dots, N\}$ . The value  $\mathbf{X}_n(t)$  is then the temperature at location  $n$  at time  $t$ . While all sensor readings are collected at finite resolutions in practice, the temperature continuously exists over time. Thus, it is natural to model and analyze  $\mathbf{X}_n(t)$  as a continuous function defined over time from the observed time points.

Over the past decades, the field of functional data analysis has seen various advances in functional data modeling, clustering, differential analysis, and outlier detection. The functional non-parametric statistics with free-modeling ideas were popularized by Ferraty and Vieu [6]. Ramsay and Silverman [33] applied parametric statistics, such as linear regression, principal components analysis, linear modeling, and canonical correlation analysis, to the functional domain. Horvath and Kokoszka [13] developed statistical methods and theory for inference (e.g., two-sample inference, change point analysis, and tests for dependence) of independent and identically distributed functional data as well as dependent functional data structures.

Besides various FDA methods, functional principal component analysis (FPCA) is one of the most classic and popular methods. The fundamental concept of FPCA includes capturing the principal directions of modes of variations along with dimensionality reduction. Using the basis spanned by the principal component, FPCA is able to summarize subject-specific features. Karhunen [16] and Loeve [23] made the first advancements in FPCA through theories on optimal data expansion of a continuous stochastic process. Building on this work, Rao [34] worked on statistical tests for the comparison of temporal growth curves. Following works on FPCA investigated its properties and improved on methodology and convergence rates [11]. Through continued systematic research on FPCA, several extensions and modifications of FPCA have been popularized, as listed in the survey by Shang [36]. Some of the practical applications of FPCA include functional magnetic resonance imaging (fMRI) [43], age-specific mortality rates [14], and analysis of income density curves [19].

Since functional data inherently consists of smooth, continuous

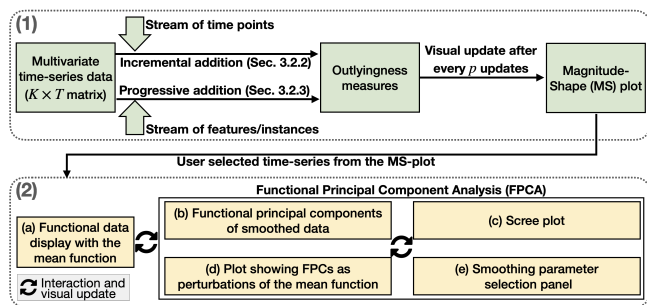


Figure 1: General architecture of our visualization tool.

sequences being collected from various sources, outlier detection is often performed as a preliminary step in analysis to distinguish sequences that follow different functions from the others. The depth of a point shows how deep a point is relative to a given data set by measuring its centrality with respect to the other points forming the data cloud. Statistic depth is a widely used non-parametric inference method (methods that make no assumptions about the probability distributions of the variables being assessed) for exploratory analysis of functional data. The concept of data depth was first proposed by Tukey [39] for visualizing bivariate data. Some of the popular depth measures include half-space depth [39], projection-depth [46], and spatial depth [42].

Several visualization tools have been developed for FDA, which serve as an effective way to communicate underlying characteristics otherwise not apparent through summary statistics and models. Hyndman and Shang [15] introduced tools to visualize large amounts of functional data, such as functional versions of bagplots (multidimensional boxplots), and highest-density-region plots. Some other popular tools include functional boxplots [39], and magnitude-shape (MS) plots [4]. The MS plot is designed to be used for visual identification of outliers by depicting the magnitude and shape outlyingness of each series of functional data. With simulated and real-world examples, the authors have shown how the MS plot is superior in identifying potential outliers. We enhance the MS plot for streaming data analysis by providing incremental and progressive algorithms to enable timely visualization updates.

## 3 METHODOLOGY

This section describes the architecture of our visual analytics tool and back-end analysis methods.

### 3.1 Architecture Overview

Fig. 1 shows the general architecture of our visual analytics tool. The tool can be divided into two main components: (1) generation of the MS plot from streaming feed and (2) interactive analysis over the generated MS plot with the auxiliary visualizations from other FDA methods, including FPCA and smoothing functions.

To make explanations concise and concrete, we describe our algorithms and analyses with streaming, multivariate time-series data as an example of functional data. While streaming, multivariate time-series data is our main analysis target, our approach can be applied to the other type of functional data as its base is general FDA methods such as the MS plot and FPCA. Here we denote the numbers of existing time points and time-series in current multivariate time-series data with  $T$  and  $K$ , respectively.

In Fig. 1-(1), we first initialize the magnitude and shape outlyingness measures by computing them from the current set of functional data. As shown in Fig. 1-(1), data updates from the stream can be the addition of either time point (i.e.,  $T \rightarrow T + 1$ ) or feature ( $K \rightarrow K + 1$ ). Based on the updates, we compute the directional outlyingness measures [4] incrementally for the addition of a time point and progressively to add a feature/instance.

While we update the outlying measures for every time point addition, for the new addition of functions—which we sometimes

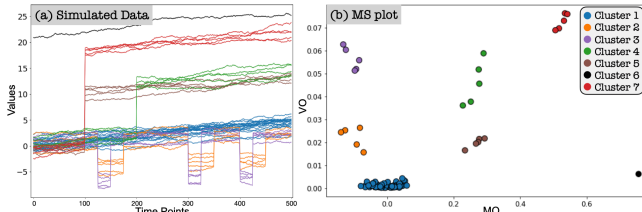


Figure 2: Visual outlier detection with the MS plot: (a) the simulated functional data and (b) the MS plot with magnitude outlyingness (MO) and variational outlyingness (VO) along  $x$ - and  $y$ -axes, respectively.

refer to as features, we perform either incremental updates with approximations, involving errors within a predefined error threshold, or progressive updates to the entire dataset if the error crosses the error threshold. We make sure that incremental and progressive updates do not overlap to avoid erroneous results.

The results are then plotted on the MS plot. An example of the MS plot can be seen in Fig. 2-b. For an incoming stream rate of every 0.5 second, we plot the results after 5 seconds, i.e., every 10 addition of time points. This is to help analysts maintain their mental map while avoiding large information loss.

The user interaction in MS plot allows the users to lasso over features/instances, and the selected data is processed in Fig. 1-(2), the FPCA pipeline. The pipeline includes (a) plotting the selected functional data and (b-e) showing FPCA results and settings: (b) the plot of functional principal components (FPCs), (c) the scree plot, (d) the plot showing FPCs as the perturbation to the mean function, and (e) the smoothing parameter settings. Sect. 3.3 describes the detail of each of these plots.

### 3.2 Incremental and Progressive Generation of the Magnitude-Shape Plot

Here we describe our algorithms<sup>1</sup> and system implementations that are designed to generate the MS plot from data streams (Fig. 1-(1)).

#### 3.2.1 Magnitude-Shape (MS) Plot

We provide a brief introduction to the MS plot [4], which we use as a main visual analysis tool and extend to be used in a streaming setting. To visually identify outliers, as shown in Fig. 2, the MS plot depicts two different outlyingness measures: mean directional outlyingness (MO) and variation of directional outlyingness (VO) [3], which represent how much a function (i.e., time-series) has a different magnitude and shape with the other functions, respectively.

A function can be considered an outlier if it behaves in a manner inconsistent with the other functions. One of the measures of the outlyingness of functions is the Stahel-Donoho outlyingness [46]. This measure is suited to the case when attribute values in time-series data roughly follow elliptical distributions; however, it cannot capture the outlyingness well when they have skewed distributions. To address this limitation, Dai and Genton [4] introduced the directional outlyingness, which they also utilize for the MS plot.

The directional outlyingness is computed by splitting the data into halves around the median and using the robust scale estimator to handle any skewness. The directional outlyingness  $\mathbf{O}$  is defined by:

$$\mathbf{O}(\mathbf{X}(t), F_{\mathbf{X}(t)}) = \left\{ \frac{1}{d(\mathbf{X}(t), F_{\mathbf{X}(t)})} - 1 \right\} \cdot \mathbf{v}(t) \quad (1)$$

where  $\mathbf{X}(t)$  is a  $K$ -dimensional function defined on a time domain  $\mathcal{T}$ ,  $F_{\mathbf{X}(t)}$  is a probability distribution of  $\mathbf{X}(t)$ ,  $d$  ( $d > 0$ ) is a depth function which decides ranks of functional observations from most outlying to most typical,  $(\cdot)$  denotes the Hadamard product, and  $\mathbf{v}(t)$  is the unit vector pointing from the median of  $F_{\mathbf{X}(t)}$  to  $\mathbf{X}(t)$ , i.e., with  $\mathbf{Z}(t)$ , the unique median of  $F_{\mathbf{X}(t)}$ ,  $\mathbf{v}(t) = (\mathbf{X}(t) - \mathbf{Z}(t)) / \|\mathbf{X}(t) - \mathbf{Z}(t)\|_2$  ( $\|\cdot\|_2$  denotes the L2-norm). Dai and Genton [4] use the projection

<sup>1</sup>The related source code will be released upon publication.

depth as a default depth function  $d$ . Note that our incremental and progressive algorithms also employ the projection depth to follow their default. The projection depth (PD) is defined as:

$$\text{PD}(\mathbf{X}(t), F_{\mathbf{X}(t)}) = \frac{1}{1 + \text{SDO}(\mathbf{X}(t), F_{\mathbf{X}(t)})}, \quad (2)$$

$$\text{SDO}(\mathbf{X}(t), F_{\mathbf{X}(t)}) = \frac{\|\mathbf{X}(t) - \mathbf{Z}(t)\|}{\text{median}(\|\mathbf{X}(t) - \mathbf{Z}(t)\|)} \quad (3)$$

where SDO is the Stahel-Donoho outlyingness [46] stated above. Now, we can define three measures of directional outlyingness:

· Mean directional outlyingness (MO):

$$\mathbf{MO}(\mathbf{X}, F_{\mathbf{X}}) = \int_{\mathcal{T}} \mathbf{O}(\mathbf{X}(t), F_{\mathbf{X}(t)}) w(t) dt \quad (4)$$

· Variation of directional outlyingness (VO):

$$\text{VO}(\mathbf{X}, F_{\mathbf{X}}) = \int_{\mathcal{T}} \|\mathbf{O}(\mathbf{X}(t), F_{\mathbf{X}(t)}) - \mathbf{MO}(\mathbf{X}, F_{\mathbf{X}})\|_2^2 w(t) dt \quad (5)$$

· Functional directional outlyingness (FO):

$$\begin{aligned} \text{FO}(\mathbf{X}, F_{\mathbf{X}}) &= \int_{\mathcal{T}} \|\mathbf{O}(\mathbf{X}(t), F_{\mathbf{X}(t)})\|_2^2 w(t) dt \\ &= \|\mathbf{MO}(\mathbf{X}, F_{\mathbf{X}})\|_2^2 + \text{VO}(\mathbf{X}, F_{\mathbf{X}}) \end{aligned} \quad (6)$$

where  $w(t)$  is a weight function defined on  $\mathcal{T}$ . Dai and Genton [4] use a constant weight function, i.e.,  $w(t) = \{\lambda(\mathcal{T})\}^{-1}$  where  $\lambda(\cdot)$  represents the Lebesgue measure.

The MS plot is a 2D scatterplot that shows, for each function (i.e., one time-series), the corresponding MO and VO as  $x$ - and  $y$ -coordinates, respectively. As shown in Fig. 2, we can visually identify the functional outliers with the MS plot. MO and VO show the outlyingness in magnitude and shape. Thus, the central functions (i.e., functions similar to the other majority of functions) are mapped the region with small  $|\text{MO}|$  and small VO (e.g., Cluster 1 in Fig. 2). On the other hand, outliers that take different magnitudes from the others across time are located in the region with large  $|\text{MO}|$  and small VO (e.g., Cluster 6). Similarly, outliers that have a different curve shape from the others are placed in the region with small  $|\text{MO}|$  and large VO (e.g., Cluster 3). When functions (i.e., points in the MS plot) have large  $|\text{MO}|$  and large VO (e.g., Cluster 7), those functions are the curves with greatly outlying in both magnitude and shape.

#### 3.2.2 Incremental Updates of the MS Plot along Time

Even though the MS plot is generated with MO and VO defined with continuous functions, in practice, MO and VO need to be computed with a finite but large number of time points. As the number of time points becomes larger, more computations are required. Consequently, when newly measured time points are continually fed from the data stream, the MS plot generation gradually becomes infeasible in real-time. To solve this issue, we derive equations that enable incremental updates of MO and VO. Our incremental updates provide *exact* MO and VO without any estimation. Using the projection depth as a depth function, the discretized versions of Eq. 1, 4, and 6 are:

$$\mathbf{O}(\mathbf{X}_t^T) = \frac{\|\mathbf{X}_t^T - \mathbf{Z}_t^T\|}{\text{median}(\|\mathbf{X}_t^T - \mathbf{Z}_t^T\|)} \cdot \frac{\mathbf{X}_t^T - \mathbf{Z}_t^T}{\|\mathbf{X}_t^T - \mathbf{Z}_t^T\|_2} \quad (7)$$

$$\mathbf{MO}^T(\mathbf{X}^T) = \sum_{t=1}^T \mathbf{O}(\mathbf{X}_t^T) w_t^T, \quad (8)$$

$$\text{FO}^T(\mathbf{X}^T) = \sum_{t=1}^T \|\mathbf{O}(\mathbf{X}_t^T)\|_2^2 w_t^T \quad (9)$$

where  $T$  is the number of time points available so far and superscript  $T$  over each symbol represents that each measure is defined on a time range  $[1, T]$ . In addition, now  $\mathbf{Z}_t^T$  is simply the median of  $K$  attributes of  $\mathbf{X}_t^T$  for each time step  $t$ . Also, here we assume  $T$  time points have an approximately constant time interval. To follow the default weight function by Dai and Genton [4], we also use a

constant weight function as  $w_t^T$ . In the discretized case,  $w_t^T = 1/T$ .

When adding a new time point at  $T + 1$ , Eq. 8 and Eq. 9 become:

$$\begin{aligned} \mathbf{MO}^{T+1}(\mathbf{x}^{T+1}) &= \sum_{t=1}^{T+1} \mathbf{o}(\mathbf{x}_t^{T+1}) w_t^{T+1} \\ &= \frac{1}{T+1} \left( T\mathbf{MO}^T(\mathbf{x}^T) + \mathbf{o}(\mathbf{x}_{T+1}^{T+1}) \right), \end{aligned} \quad (10)$$

$$\begin{aligned} \mathbf{FO}^{T+1}(\mathbf{x}^{T+1}) &= \sum_{t=1}^{T+1} \left\| \mathbf{o}(\mathbf{x}_t^{T+1}) \right\|_2^2 w_t^{T+1} \\ &= \frac{1}{T+1} \left( T\mathbf{FO}^T(\mathbf{x}^T) + \left\| \mathbf{o}(\mathbf{x}_{T+1}^{T+1}) \right\|_2^2 \right). \end{aligned} \quad (11)$$

Then, because of Eq. 6,  $\mathbf{VO}^{T+1} = \mathbf{FO}^{T+1} - \left\| \mathbf{MO}^{T+1} \right\|_2^2$ . When computing  $\mathbf{MO}^{T+1}$  and  $\mathbf{FO}^{T+1}$ , we have already obtained  $\mathbf{MO}^T$  and  $\mathbf{FO}^T$ . Thus, to obtain  $\mathbf{MO}^{T+1}$  and  $\mathbf{FO}^{T+1}$ , we need to only calculate the directional outlyingness  $\mathbf{O}$  for the newly added time point, which has time complexity  $\mathcal{O}(K)$  when using the PD as a depth function. Also, because  $\mathbf{FO}^T$  and  $\mathbf{VO}^T$  are scalars and  $\mathbf{MO}^{T+1}$  are a  $K$ -length vector, the required memory space to save the previous result is  $\mathcal{O}(K)$ . Therefore, we can update the exact values of the three measures of directional outlyingness with small time and space complexities that do not relate to the increasing number of time points,  $T$ . Note that while the equations above are for the incremental addition, as seen in Eq. 10 and Eq. 11, the incremental deletion is also supported, which can be derived with minor adjustments of signs, etc.

### 3.2.3 Progressive Updates of the MS Plot along Features

When the number of functions (or the number of attributes of one function)  $K$  in a system is large, computation of the directional outlyingness measures with the way in Sect. 3.2.1 can be a huge overhead. Also, when analysts want to add new functions into the MS plot to analyze with the former functions (e.g., adding temperatures obtained from different compute racks), the original algorithm in Sect. 3.2.1 requires computation for all functions—including new and old functions. To provide useful intermediate results or enable the incremental addition of features, we design a progressive algorithm that generates the MS plot with estimated directional outlyingness measures. Also, our algorithm provides a refinement mechanism to avoid having a low quality MS plot.

Unlike incremental updates along time (Sect. 3.2.2), when adding new features, we cannot obtain exact solutions while keeping the time complexity constant in terms of an increase in the number of features. This is because all computations are related to  $\mathbf{Z}_t^T$  (the median of  $K$  attributes in  $\mathbf{X}_t^T$ ); thus, the update of  $\mathbf{Z}_t^T$  based on a new function requires recomputation of the measures for all functions at all time points. Therefore, we (1) incrementally update the results by assuming  $\mathbf{Z}_t^{T,K+1} \approx \mathbf{Z}_t^{T,K}$  (superscript  $K$  shows the corresponding measure is defined on  $K$  features) as long as the errors are within the predefined error threshold and (2) progressively update the results with  $\mathbf{Z}_t^{T,K+1}$  if the predefined error threshold is crossed. The condition  $\mathbf{Z}_t^{T,K+1} \approx \mathbf{Z}_t^{T,K}$  is checked using the Kullback–Leibler divergence (KL) [21] of the mean absolute deviation between the new feature and the original features. Since KL divergence values can range anywhere between 0-infinity, we have set the error threshold 10 by default, and this can be varied by the user.

Let  $\mathbf{Y}^T \in \mathbb{R}^{1 \times T}$  be a new feature adding to  $\mathbf{X}^T$ . For  $\mathbf{Y}^T$ , with the assumption of  $\mathbf{Z}_t^{T,K+1} \approx \mathbf{Z}_t^{T,K}$ , we can compute SDO and  $\mathbf{v}_t^T$  with:  $\text{SDO}(\mathbf{Y}_t^T) \approx |\mathbf{Y}_t^T - \mathbf{Z}_t^{T,K}| / \text{median}(|\mathbf{Y}_t^T - \mathbf{Z}_t^{T,K}|)$  and  $\mathbf{v}_t^T \approx (\mathbf{Y}_t^T - \mathbf{Z}_t^{T,K}) / \|\mathbf{Y}_t^T - \mathbf{Z}_t^{T,K}\|_2$ . With these values, we can compute  $\mathbf{O}$  and  $\mathbf{MO}^T$  for  $\mathbf{Y}^T$  with Eq. 7 and 8. Afterward, we can obtain

$\mathbf{MO}^{T,K+1}$  and  $\mathbf{FO}^{T,K+1}$  (i.e., updated  $\mathbf{MO}$  and  $\mathbf{FO}$  with  $\mathbf{Y}^T$ ) with:

$$\mathbf{MO}^{T,K+1} = \begin{bmatrix} \mathbf{MO}^{T,K} \\ \mathbf{MO}^T(\mathbf{Y}^T) \end{bmatrix} \quad (12)$$

$$\mathbf{FO}^{T,K+1} = \mathbf{FO}^{T,K} + \mathbf{FO}^T(\mathbf{Y}^T) \quad (13)$$

When adding a new function, there is a good possibility that the function may closely represent the shape and magnitudes of the existing functions. Therefore, by avoiding updating  $\mathbf{Z}$  for each addition of a function, we significantly reduce the computational overhead. However, as stated above, once the difference between  $\mathbf{Z}_t^{T,K}$  and  $\mathbf{Z}_t^{T,K+1}$  becomes larger than the threshold, our algorithm starts to recompute the measures for each function one by one. Similar to the incremental update in Sect. 3.2.2, the deletion of features is also supported with minor changes in the above equations.

### 3.2.4 Implementation with Visual and Computational Considerations on Update Frequency

In the general architecture of our visual analytics tool, our implementation allows for the processing of incoming time points from the data stream and the addition of new features. On top of this capability, we implement our tool with the design recommendations for progressive visual analytics systems by Turkay et al. [40]. In case of receiving a new time point, we update the outlyingness measures at each time step in the back-end. However, the MS plot is not updated at every addition of a time step; instead, we update it at a predefined number of arrived time points (we set 10 time points as a default). When receiving a new feature, we update both the outlying measures and the MS plot. This procedure adds a new point to the MS plot. When  $\mathbf{Z}_t^{T,K+1} \approx \mathbf{Z}_t^{T,K}$ , the outlyingness measures no longer give reasonable results. Hence, the previously computed measures need to be updated with  $\mathbf{Z}_t^{T,K+1}$ . This update can be computationally expensive to be done on the fly if the dataset size is large. Therefore, we compute the results asynchronously in the back-end, and the front-end visualization is updated on completion. Additionally, all visual updates are performed with animated transitions for better interpretation support of changes.

### 3.3 Reviewing the MS Plot with Auxiliary Information and Functional Principal Component Analysis

Fig. 3 shows the user interface (UI) of our visual analytics tool. It consists of the (a) MS plot view, (b) space view, (c) data view, (d) the FPCA views. The analysis with the tool starts from the selection in the space view. The space view shows the related spatial information to the data if such information is available. For example, in Fig. 3, we analyze multiple temperatures measured at each compute rack in a supercomputer—each rack has 180 temperature sensor measurements. Thus, in Fig. 3-b, we visualize the rack location information, and using the orange sequential colormap, we color-code the number of outlier temperature readings, which are identified in the MS plot. With mouse actions (mouse-clicking or lasso selection), the analysts can select items of interest from the space view (i.e., racks in Fig. 3-b), and then the UI shows the related points in the MS plot. An example in Fig. 3 selects the dark orange color cell (i.e., the rack contains many outliers) around the top center (“o40”).

For the related points (i.e., temporal curves), the MS plot view shows the up-to-date MS plot, which is generated with the method described in Sect. 3.2. Additionally, we color plotted points by its membership in either central or outlying curves (teal: central, pink: outlying curves). Here, as a default, we define the central curves as curves that have MO within 25-75% of the value range and VO below than 75% of the value range). Again, the MS plot allows analysts to select points of interest with mouse actions to see the detailed information in the other views (Fig. 3-c, d). The selected points are indicated with bigger brown circles.

Fig. 3-c visualizes the selected points as line charts. In addition, to cover the typical central curve, we visualize their mean function—

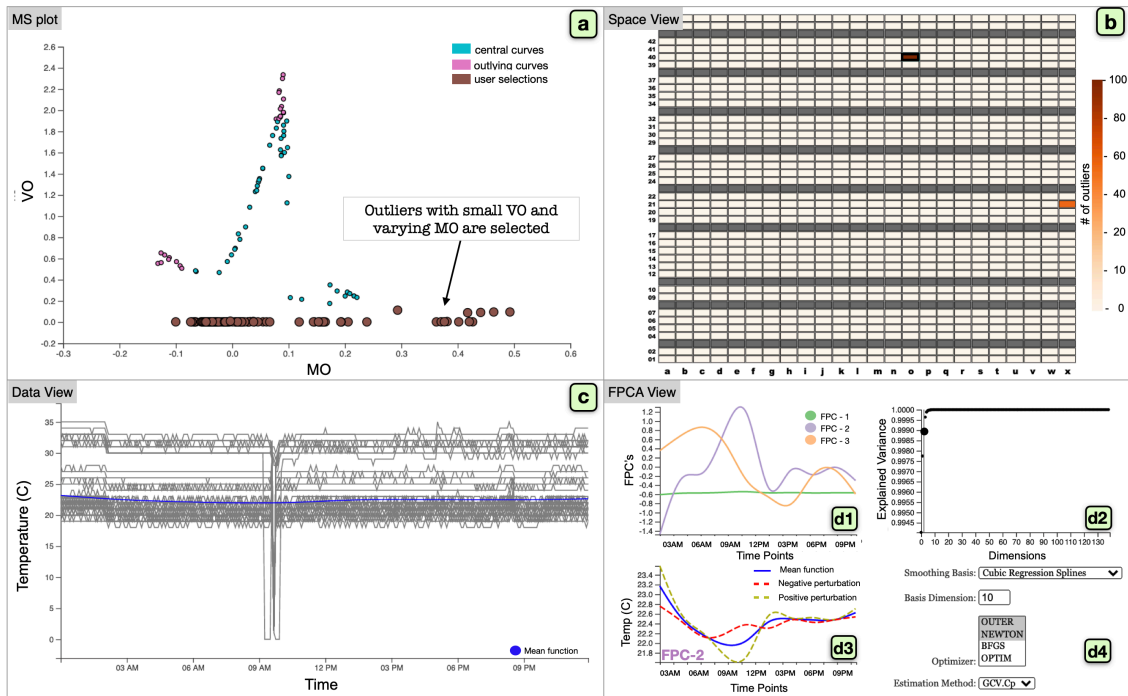


Figure 3: The user interface of our visual analytics tool. (a) The MS plot view shows MO and VO measures as a scatterplot, which is being updated incrementally and progressively. (b) The space view provides the related spatial information if available (here shows the compute rack information). (c) The data view depicts the time-series selected in the MS plot. (d) The FPCA views display the FPCA results and settings, which include: (d1) FPC plot, (d2) scree plot, (d3) FPC as a perturbation of the mean plot, and (d4) functional smoothing parameter selection panel.

a smoothed line around their mean at each time point—as a blue line. These visualized lines can be further analyzed with the FPCA views (Fig. 3-d).

To apply FPCA [44] on the lines shown in Fig. 3-c, we first need to apply smoothing to the lines. Fig. 3-d4 allows analysts to select the smoothing basis functions, the number of basis, the method for optimizing the smoothing parameter, and the smoothing parameter estimation method [12]. We show the default settings in Fig. 3-d4. Then, FPCA is performed on the smoothed lines, and functional principal components (FPCs) are generated, as shown in Fig. 3-d1. Analogous to PCA, FPCs preserve the variance of functions as much as possible by defining a weight for each time point in a continuous curve. By looking at the shape of each FPC, we can understand which time has a strong influence on each FPC. For example, in Fig. 3-d1, the first FPC (FPC-1) has the same weight around -0.6 across time, while the second FPC (FPC-2) has a large weight around 9 AM. Because most of the lines are relatively flat in Fig. 3-c, FPC-1 seems to preserve the major variance related to all time points; FPC-2 seems to preserve the variance related to the distinct valley around 9 AM in Fig. 3-c. This can be further confirmed by our selection method of time-series that relate to each FPC. When analysts select one FPC from Fig. 3-d1, for each time-series, we compute the FPC score [44], which represents how strongly the time-series relate to the corresponding FPC. Then, the tool select and highlight the top- $k$  ( $k = 10$  by default) time-series that highly relate to the selected FPC. The corresponding points are also highlighted in Fig. 3-a. As shown in this example, FPCA is useful to identify the influential time from FPCs and categorize time-series with FPCs.

While the top-3 FPCs are shown in the FPC view by default, analysts can use the scree plot (Fig. 3-d2) to select the number of FPCs to be shown. Similar to ordinary PCA, it shows the number of dimensions (or components) and the cumulative explained variance ratio. From this, analysts can judge how many principal components are required to reasonably capture the variance in the data.

In the FPC as a perturbation of the mean plot (Fig. 3-d3), we plot the mean function of the selected data (the same one in Fig. 3-c

but with a different y-range) and the functions obtained by adding and subtracting a suitable multiple,  $\sqrt{2\xi_i}$ , of an FPC chosen from the FPC plot, FPC- $i$  [33], where  $\xi_i$  is the eigenvalue corresponding to FPC- $i$ . The obtained functions are shown as positive and negative perturbations, respectively. This explains the fluctuation of the measured data (i.e., y values in Fig. 3-d3) the FPC- $i$  captures. For example, in Fig. 3-d3, where FPC-2 is selected, the positive perturbation has a clear drop from the mean function around the 9 AM while it has a slight rise around 3 AM. This indicates that time-series highly related to FPC-2 are mainly characterized by their clear drop around 9 AM, which can be confirmed with Fig. 3-c.

By showing only the selected time-series and their FPCA results, we can reduce not only visual clutter in visualization but also computational costs of FPCA, which generally has a high computational complexity as with the other FDA methods. This procedure also can extract more useful FPCA results that closely relate to time-series of interest rather than extracting FPCs from the entire data.

Here we summarize findings from the interactive analysis above. From Fig. 3-b, we find 2 racks (“o40” and “x21”) that behave abnormally and select “o40” since it includes more outliers. Then, from the MS plot, we further select time-series that have low VO but have varying MO. Indeed, from Fig. 3-c, we can see that while all the time-series have similar magnitudes across time, there is a significant dip in the temperature soon after 9 AM. By applying FPCA to the selected time-series, we extract FPCs and the modes of variation. Especially, we see that FPC-2 captures the variation related to the dip, as seen in Fig. 3-d1, d3. The perturbation plot of FPC-2, captures readings that flip across the mean close to 9:00AM and there is another flip across the mean after 9:30AM in the duration of the failure. We provide further details of the analysis and the dataset in Sect. 4.3.

## 4 CASE STUDIES

We have shown an analysis example in Sect. 3.3. We further demonstrate the effectiveness of our tool with three case studies, including analyses of the Canadian weather, ozone level, and supercomputer’s

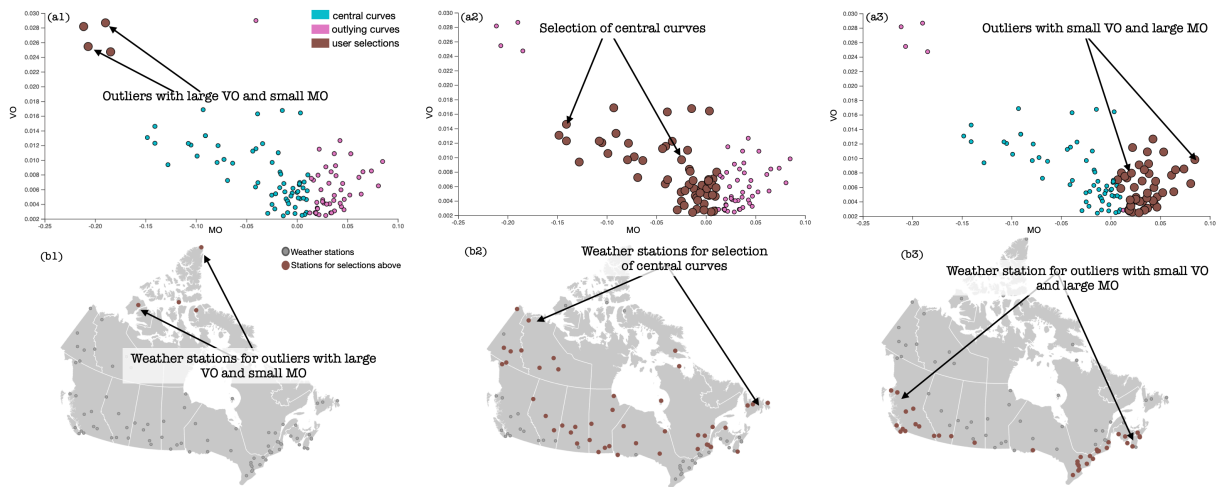


Figure 4: The characterization of Canadian Weather with the MS plot. (a1, a2, a3) show the different selections of the weather stations performed in the MS plot. (b1, b2, b3) show the corresponding weather stations.

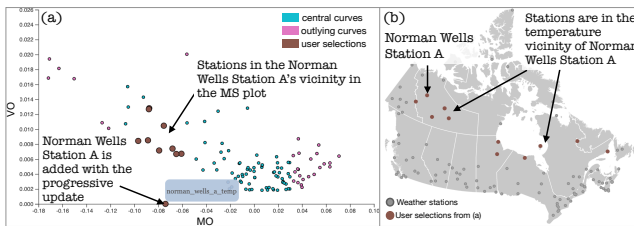


Figure 5: The results after the progressive update in the MS plot, which adds a series of temperature readings at a new station, Norman Wells Station A. From the MS plot (a), we select the new station and the stations placed close to the new station in the MS plot. (b) shows the corresponding stations in brown.

hardware log datasets. Each dataset is preprocessed to handle missing values and to extract relevant information for the analysis <sup>2</sup>.

#### 4.1 Study 1: Analysis of Canadian Weather Data

We analyze the historical climate data in Canada [9]. We filter the data by province/territory, weather stations, and the time period. We choose 118 stations for the years 2019 and 2020. The dataset consists of daily measurements of temperature, precipitation, wind speed, rain days, etc., along with minimum, maximum and average values. Here we show how the MS plot characterizes the readings, specifically temperature measurements. We then illustrate the results from the incremental and progressive updates on the MS plot.

As shown in Fig. 4-a1, after updates in a period of time, the MS plot starts to reveal several outliers. We select two distinct groups of outliers and central curves in Fig. 4-a1, a2, a3. Fig. 4-b1, b2, b3 show the corresponding stations visualized in the space view. In Fig. 4-a1, we select outliers that have large VO and small MO. Fig. 4-b1 shows these stations (Arctic Bay, Resolute, Thomson River, and Alert) lie in the far north region of Canada, each of which has bitterly cold temperatures during the winter and high temperatures of up to 20 °C during the summer. On the other hand, from Fig. 4-a2, b2, the stations that have the central curves are located in the central regions of Canada. At these locations, the summer is usually warm with temperatures range from 15 °C in May to the mid-30 °C in July and August while the winter normally begins in November and temperatures generally remain below the freezing point. In Fig. 4-a3, b3, we select measurements with high magnitude and low variational outlyingness. The low variational outlyingness tells us that the weather in these stations do not show large fluctuations when compared to the central curves. The corresponding

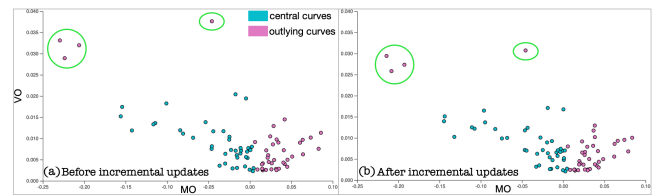


Figure 6: The MS plot (a) before and (b) after the incremental updates. From (a) generated with temperatures for 300 days, 20 additional days are added in (b). Both (a) and (b) have similar distributions of point positions. However, each point's VO tends to be smaller in (b). This is more salient in the high VO outliers indicated with the green circles.

stations are in the southwest and southeast regions of Canada, which are characterized by temperature typically varying from  $-7.2^{\circ}\text{C}$  to  $28.3^{\circ}\text{C}$  and is rarely below  $-16.6^{\circ}\text{C}$  or above  $33.8^{\circ}\text{C}$ . For the above observations, we can see that the MS plot characterize the temperatures at the different stations well, and successfully identify the outliers, especially the stations selected in Fig. 4-a1, where the temperature has excessively low magnitudes and high variations.

We illustrate an analysis with the progressive update in Fig. 5. As described in Sect. 3.2.3, the progressive update is performed with the assumption in the medians  $\mathbf{Z}_{K+1} \approx \mathbf{Z}_K$  as long as the difference falls within the error threshold. With this assumption, the MS plot produces a sufficient result while avoiding significantly high computational cost. In Fig. 5-a, under the assumption above, the MS plot places the newly added temperatures measured at Norman Wells Station A. The new point in the MS plot is at the lower central region slightly away from the rest of the points. We select the new point and additional points close to it to see if the placement of the new station makes sense. From Fig. 5-b, all selected stations, shown in brown colors, lie in the spatial and temperature vicinity of the newly added feature corresponding to Norman Wells Station A. Therefore, we see that although the newly added station introduces some errors, these errors are not significant. Also, if these errors cross the error threshold, our back-end mechanism asynchronously updates the results with the exact value of  $\mathbf{Z}^{K+1}$  for the entire dataset.

We also demonstrate an analysis with the incremental update in Fig. 6. Fig. 6-a shows the MS plot generated with the temperatures measured at the first 280 days at 100 stations. Then, we keep observing the MS plot until the temperatures in additional 20 days in October are added (Fig. 6-b). Note that the incremental updates of time points does not cause additional errors unlike the progressive updates. From Fig. 6-a, b, we see that the distribution of points in the MS plot is not changed much before and after the updates. This is expected since the temperatures did not widely fluctuate within

<sup>2</sup>The datasets in Studies 1 and 2 will be released online upon publication.

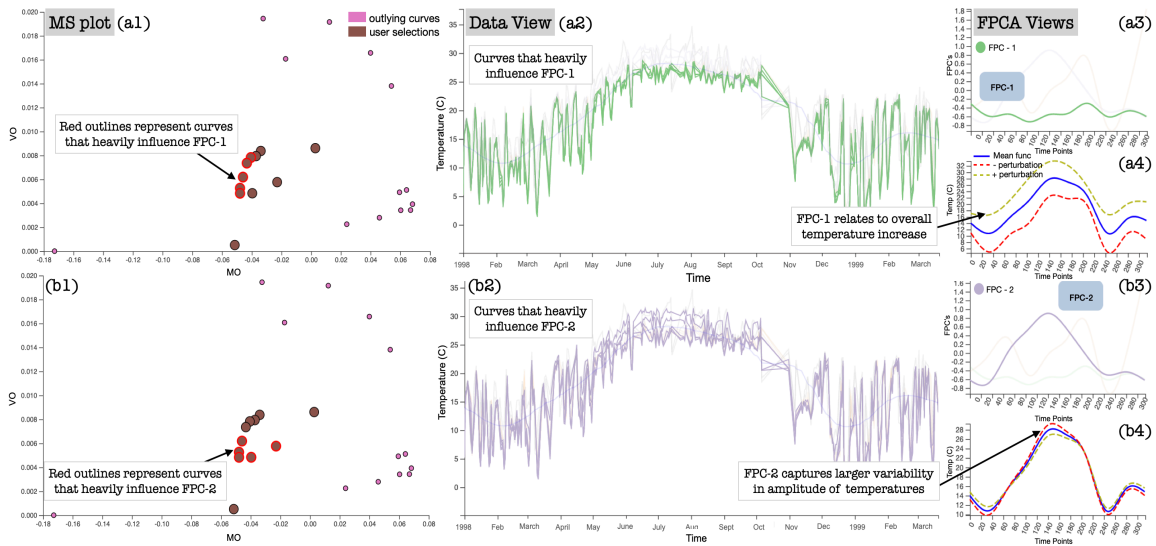


Figure 7: The in-depth analysis of central curves identified by the MS plot. The figure shows (1) MS plot is displayed on the left, (2) the Ozone temperature curves in the middle, and (3) the FPCA analysis (consisting of FPC's and FPC as perturbations of mean) plots in the right

these 20 days. However, at the same time, we can see that each point's VO becomes slightly smaller in Fig. 6-b. Especially, for the outliers with high VO—highlighted with green circles, this tendency can be seen more clearly. We can consider that this smaller change is caused by stable temperatures in October across Canada.

## 4.2 Study 2: Analysis of Ozone Level Data

Ozone levels in the air fluctuates due to some related parameters (e.g., temperatures) which is often the case with a stochastic process. When the fluctuations cross a certain threshold, it results in adverse effects on human health. Hence, it is crucial to accurately monitor these parameters and issue a warning of a dangerous level. The ozone dataset contains 75 features which include temperature, wind speeds, ozone background level, and relative humidity each measured at multiple geo-potential heights at different times of the day. Here, we analyze temperatures measures at various heights on the ozone layer. The results generated with our tool is shown in Fig. 7.

In this case study, we demonstrate the usefulness of the analysis with FPCA to supplement or improve the MS plot. While the MS plot in Fig. 7-a1 reveals clear outliers, here we analyze the central curves in detail. We first select the central curves from the MS plot, as shown with brown circles in Fig. 7-a1. With the help of FPCA, we can categorize subgroups of these central curves and see how these individual subgroups vary from the others. Fig. 7-a3 shows the FPCA result of the selected central curves. While the FPCA result originally depicts the top-3 FPCs, we individually select the first and second FPCs (FPC-1 and FPC-2). Then, the related information is highlighted in all views.

We first select FPC-1 from the FPC plot, as shown in Fig. 7-a3; then related central curves are highlighted with the red outlines in a1 and emphasized with the corresponding FPC color in a2. In Fig. 7-a4, the mean function is visualized with its positive and negative perturbations. From Fig. 7-a2, we see that all curves related to FPC-1 have the same fluctuation patterns (i.e., most of them are heavily overlapped at every time point). In Fig. 7-a4, by looking at the difference between the mean function and its positive or negative perturbation, we can see that the effect from FPC-1 is merely to add and subtract a constant throughout the entire duration.

When we select FPC-2 in Fig. 7-b3, Fig. 7-b4 accounts for overall variability in the temperature amplitudes in the entire duration of measurement. The perturbations (shown in dotted red/yellow lines) show that the related curves flip across the mean at around time point 80, and there is another flip at around time point 200. The captured variability is also seen in Fig. 7-b2. Therefore, FPC-2 accounts for

larger amplitude fluctuations in the readings over the time period of the measurements. The corresponding curves are also highlighted in the MS plot with the red outlines Fig. 7-b1. Hence, with this example, we find interesting patterns in variations within a group, which would have otherwise gone unnoticed. Once these patterns are identified, it could be modeled to detect similar patterns in the MS plot. For example, by adjusting weight  $w_i^T$  assigned to each time point for computing MO and VO, we can make the MS plot more sensitive to value changes in the corresponding time periods (e.g., 120 – 200 in the above case).

## 4.3 Study 3: Analysis of Supercomputer Hardware Logs

We analyze rack environment logs obtained from a supercomputer. Rack environment logs provide information collected from various sensors housed in the compute rack subsystem (system board, air/water cooling, power supply, etc.) of a supercomputer. These logs contain readings of voltages, temperatures (water/air/CPU), fan speeds, etc. that can be utilized to find abnormalities during failure events. Therefore, studying these logs helps us understand the various underlying hardware failure patterns. These studies aid in maintaining robustness and improving reliability in large-scale machines. Thus, there have been past efforts to identify and analyze supercomputer log errors with visual analytics tools [8, 10, 37].

We specifically analyze data procured from the K computer's [26] rack environment logs on November-17th, 2017. The logs contain data from 864 compute racks, with 1,163 different sensor measurements (e.g., CPU temperatures, circuit voltages, fan speeds) collected every 5 minute interval (i.e., 288 timestamps in a day). For this case study, we select to analyze temperatures collected at 180 sensors per rack. Therefore, in total, we end up with  $180 \times 288 = 51,840$  sensor measurements per rack. We have already analyzed the same data in Sect. 3.3 with the MS-plot, and we have identified different temporal patterns with FPCA. Here, we demonstrate the effect of settings of the smoothing function on FPCA in more detail.

The data collection used for FDA is usually observations gathered discretely over time at fixed or random time intervals; however, many FDA methods, including FPCA, expect input data to be gathered at fully defined trajectories, i.e., at time interval close to zero. This leads to an analysis problem with an extremely large number of time points. Therefore, to model the underlying stochastic process of the data while overcoming the curse of dimensionality, data smoothing is often applied. While the smoothing helps in regularization and elimination of unnecessary roughness or noise from the analysis, the settings related to smoothing are highly important to obtain the

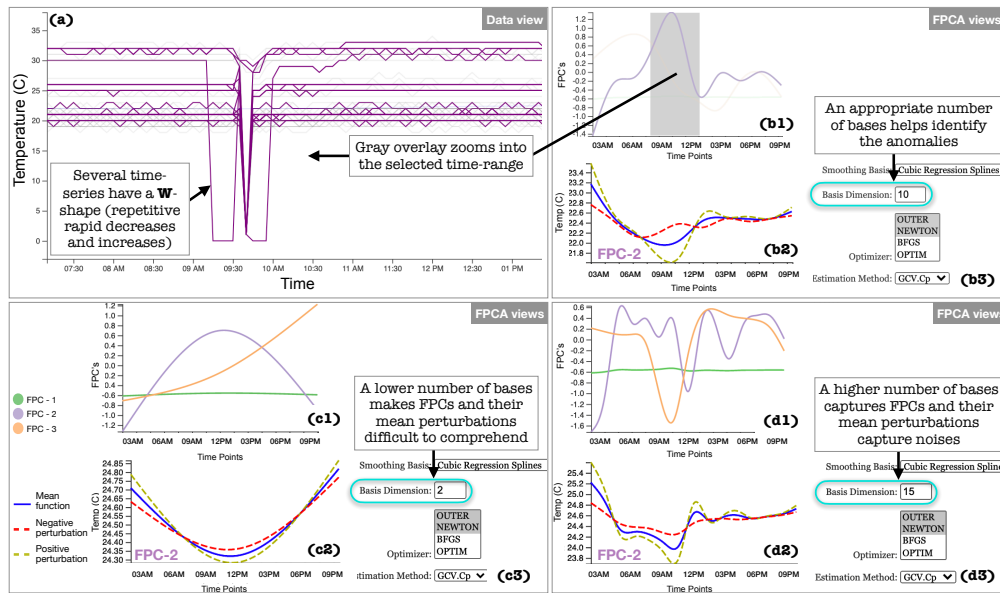


Figure 8: The effect of the number of basis functions on the FPCA results. (a) shows the data view. (b1, b2, b3) the FPCA views produced with 10 basis functions. Similarly, for (c1, c2, c3) and (d1, d2, d3), 2 and 15 are used as the numbers of basis functions, respectively.

desired FPCA results.

Fig. 8 shows how the choices in the number of basis functions used to model our dataset changes the FPCA results. In Fig. 8-b3, we choose 10 as the number of basis functions (the same setting with Fig. 3). The corresponding views are updated (b1, b2). In Fig. 8-b1, we select FPC-2, and we use the brushing tool, as shown with a gray overlay, to select the time range that shows the rapid increase in the FPC. Then, as shown in Fig. 8-a, the data view zooms into the related time range and shows a set of time-series highly related to FPC-2 within that range. Therefore, with the selection of an FPC and brushing, we can identify time-series and a time range that associate with peculiar variations on the selected FPC. However, if we use too few basis functions to model the functional phenomena, we may not effectively capture important underlying information. For example, in Fig. 8-c3, we select 2 as the number of basis functions. This choice is able to model the drop in some time-series by FPC2, as shown in Fig. 8-c2; however, this setting fails to capture the sudden drop and return, which is well modeled in Fig. 8-b1, b2. On the other hand, as shown in Fig. 8-d1, d2, d3, where the number of basis functions is 15, using too many basis functions makes FPC-2 too closely following the dataset. This implies that the smoothing function performs curve-fitting rather than smoothing and captures too much noise in our data.

The three case studies demonstrate how a combination of the MS plot and FPCA can identify not only outliers but also peculiar behaviors of data within these outliers or find missing outliers in the MS plot to improve the visual outlier detection with the MS-plot.

## 5 DISCUSSION

Fig. 9(1)-(4) compares the results of dimensionality reduction (DR) and outlier detection when using ordinary MS plot [4], incremental MS plot (Inc-MS, described in Sect. 3.2.2), incremental PCA (iPCA) [35], and UMAP [24]. We have chosen iPCA and UMAP as representative linear and nonlinear DR methods, which are often used to visually identify patterns from multiple time-series data [8, 41]. We use the supercomputer environment log, ozone temperature data, and Canadian weather data to demonstrate how each of these methods identify and capture the data's underlying stochastic process.

In the case of the supercomputer dataset, we see that UMAP and iPCA produce discernible clusters. Although most clusters can group readings with similar trends, some clusters show both normal

and abnormal readings (as shown in red circles). The MS and incremental MS plots in each case produce identical results with the incremental MS providing a boost in performance (as discussed in Sect. 3.2.2, it provides the exact solution). For the ozone temperature dataset, there are three outliers (shown in red). While the MS plots clearly isolate these outliers, UMAP fails to isolate these readings. iPCA isolates these readings, but the rest of the readings are spread apart. The Canadian weather dataset contains varying temperatures throughout the year gathered from multiple weather stations. The data was preprocessed through smoothing using B-splines with 20 bases and order 3. This produced a reasonable representation of the original data without significant information loss. In Fig. 9(1)-(4), we see that all four methods fail to produce distinct clusters for weather stations belonging to Continental and Atlantic weather types. The UMAP algorithm, with the best result for parameter set being  $n\_neighbors = 4$ ,  $min\_dist = 0.05$ , and  $metric = "correlation"$ , grouped Arctic, Atlantic, and Continental weather types in one cluster, shown inside red circle. This particular case reveals that even the best algorithms sometimes fail to capture all the underlying characteristics of a dataset. To make up for such a drawback, additional algorithms could be used in conjunction to reveal detailed underlying information. In Fig. 9(5)(6), we see how the addition of new features introduces errors due to the approximations in our progressive computations to add new features. As long as the errors are within the user-specified error threshold, the approximations can be assumed to produce close to valid results. This is seen in each of the datasets where we have added 4-5 new features. The newly added features lie in the close vicinity of the actual value.

Also, we want to note that the MS plot provides more interpretable result in characterization of time-series based on their outlyingness. Since the MS plot directly show the magnitude and shape outlyingness as  $x$ - and  $y$ -coordinates, we can immediately understand why some time-series are grouped together. On the other hand, dimensionality reduction methods such as iPCA and UMAP require additional steps to understand each revealed cluster.

In Fig. 10, we use a supercomputer hardware log data to show how the computation times compare. We scale the data starting with a data size of  $100 \times 100$  to  $10,000 \times 10,000$ . The results are computed for 10 iterations for each DR method and each data size. We then interpolate the results using a regression plot. In Fig. 10, we see for each data size incremental MS plot either gave the same performance as MS plot (when data size was in the range of few

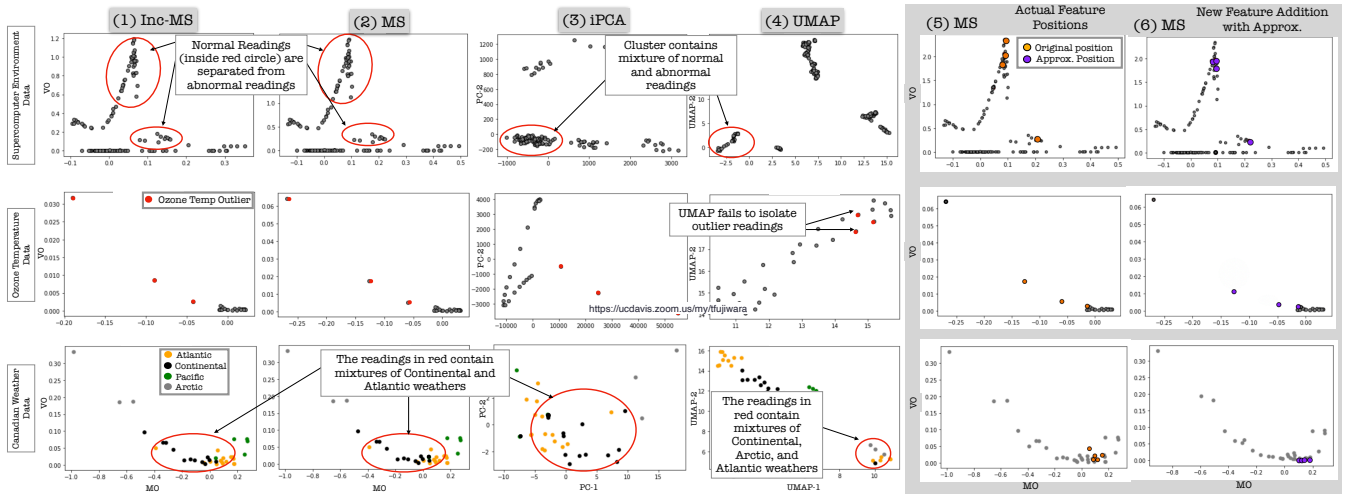


Figure 9: The comparison of results among (1) incremental MS plot, (2) MS plot, (3) iPCA, and (4) UMAP. (5) shows the actual position of features in the MS plot (in orange) without progressive feature addition, and (6) shows the progressive addition of the same features (in purple) as (5) with approximation. The dataset used include, supercomputer environment log, ozone temperature data, and Canadian weather data.

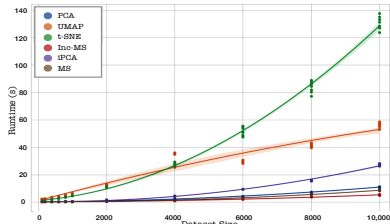


Figure 10: The comparison of completion time, showing how performance scales with dataset size.

Table 1: Completion time (in seconds) of the initial data fit and the incremental time point addition.

| Features | Time Points | Initial Fit | Incremental Fit |
|----------|-------------|-------------|-----------------|
| 1,000    | 100         | 0.0109      | 0.0009          |
| 1,000    | 1,000       | 0.0640      | 0.0011          |
| 1,000    | 10,000      | 0.5373      | 0.0013          |
| 1,000    | 20,000      | 1.3357      | 0.0010          |

Table 2: Completion time (in seconds) of the initial data fit, the progressive feature addition with and approximate results, and the progressive feature addition (PFA) without approximation.

| Features | Time Points | Initial Fit | Approx. PFA | Overall PFA |
|----------|-------------|-------------|-------------|-------------|
| 100      | 1,000       | 0.0038      | 0.0182      | 0.02391     |
| 1,000    | 1,000       | 0.0495      | 0.0374      | 0.0891      |
| 10,000   | 1,000       | 0.5910      | 0.4702      | 1.0079      |
| 20,000   | 1,000       | 1.7038      | 0.9838      | 2.5148      |

hundreds) or outperformed the traditional MS plot implementation by a factor of 2 times for a data size of  $20,000 \times 20,000$ , and 3.5 times as the data size increased to  $30,000 \times 30,000$  samples (not shown in figure). The MS and incremental MS plot implementations outperform PCA and incremental PCA (iPCA). The non-linear DR methods are computationally more expensive, as seen in the green and orange lines in Fig. 10.

Table 1 and Table 2 show the completion times (in seconds) for each computation type within the incremental MS and progressive MS methods, respectively. The completion times are the average values of 10 executions. For incremental MS computations, we first process an initial set of data consisting of varying *time points* (100, 1,000, 10,000, 20,000), and fixed number of *features/functions* (1,000). This is followed by the addition of *one* new time point, which is used to update the existing outlyingness measures incrementally. We see that as the *initial* time points are increased from 100 to 20,000, with a fixed feature size of 1,000, the incremental fit takes about 1.1ms. The completion time for initial fit increases as *time points* are increased, while the incremental step is independent of the data size. Therefore, the computation costs of adding

a new data point are low enough and aids effective online streaming analysis. For progressive MS computations, shown in Table 2, we first process an initial set of data consisting of varying *features* (100, 1,000, 10,000, 20,000), and fixed number of *time points* (1,000). This is followed by the addition of *one* new feature, which is used to update the existing outlyingness measures using the progressive methodology. In Table 2, we see that as the *initial* features are increased from 100 to 20,000, with a fixed *time point* size of 1,000, the progressive fit with approximation takes almost as long as the initial fit. Here, the bottleneck is the computation of the Kullback-Leibler divergence of the mean absolute deviation of the new feature and the original features. This computation depends on the size of the data. The completion time for progressive fit without approximation (i.e., the entire dataset result is updated) is higher as expected and is almost double the computation time as the initial fit.

Although FDA has gained more traction in recent years, discrete analysis is largely preferred over its functional counterparts. This is mainly because the analyses are computationally less expensive and are easily accessible through multiple implementations in popular programming languages. In this work, we have demonstrated how FDA in an online streaming analysis environment can help identify and capture the underlying data characteristics. With the use of FPCA, through FPC's and functional mean perturbations, we identify modes of variations within clusters over the continuum, which would have gone unnoticed using a traditional PCA.

## 6 CONCLUSION

With the advent of exascale systems and data being collected at a larger scale than before, it becomes necessary to build tools and applications that can process such data in a timely and reactive manner. Many time-dependent data are intrinsically functional in nature. Functional analysis helps reveal various characteristics in the data through derivative analysis and helps source patterns and variations that would have gone unnoticed.

We have built a visual analytics tool that processes and monitors large online time-series data using FDA. This is achieved through incremental computations of the magnitude shape outlyingness measure and progressive analysis of the addition of new functions. The progressive analysis updates an approximated result as long as the errors are within a predefined threshold. The results are re-computed promptly when this threshold is crossed, and the visualization is updated. With the incremental analysis, we are able to achieve two times the performance boost for a data set of size 20,000 time points and a performance boost of 3.5 times for a dataset of 30,000 time points. We enhance the ability to understand the underlying errors

by using functional principal component analysis (FPCA) in our pipeline. FPCA helps capture multiple modes of variation and shows which types of fluctuation (amplitude, phase shift) is captured by each identified mode.

In the future, we plan to extend our work to multivariate data, such as elastic curves. We also plan to implement incremental analysis for different depth measures.

#### ACKNOWLEDGMENTS

This research was supported in part by the U.S. National Science Foundation through grant IIS-1741536 and the Argonne National Laboratory through contract 8F-30225.

#### REFERENCES

- [1] G. Aneiros, R. Cao, R. Fraiman, C. Genest, and P. Vieu. Recent advances in functional data analysis and high-dimensional statistics. *J. multivariate analysis*, 170:3–9, 2019.
- [2] T. Crnovrsanin, J. Chu, and K.-L. Ma. An incremental layout method for visualizing online dynamic graphs. *J. Graph Algorithms and Applications*, 21(1):55–80, 2017.
- [3] W. Dai and M. Genton. Directional outlyingness for multivariate functional data. *Computational Statistics & Data Analysis*, 03 2019.
- [4] W. Dai and M. G. Genton. Multivariate functional data visualization and outlier detection. *J. Computational and Graphical Statistics*, 27(4):923–934, 2018.
- [5] A. Dasgupta, D. L. Arendt, L. R. Franklin, P. C. Wong, and K. A. Cook. Human factors in streaming data analysis: Challenges and opportunities for information visualization. *Computer Graphics Forum*, 37(1):254–272, 2018.
- [6] F. Ferraty and P. Vieu. *Nonparametric functional data analysis: Theory and practice*. Springer Science & Business Media, 2006.
- [7] T. Fujiwara, J. Chou, S. Shilpika, P. Xu, L. Ren, and K. Ma. An incremental dimensionality reduction method for visualizing streaming multidimensional data. *IEEE Trans. on Visualization and Computer Graphics*, 26(1):418–428, 2020.
- [8] T. Fujiwara, Shilpika, N. Sakamoto, J. Nonaka, K. Yamamoto, and K. Ma. A visual analytics framework for reviewing multivariate time-series data with dimensionality reduction. *IEEE Trans. on Visualization and Computer Graphics*, 2020 (early access).
- [9] Government of Canada. *Canadian Weather Historical Data*, 2019.
- [10] H. Guo, S. Di, R. Gupta, T. Peterka, and F. Cappello. La VALSE: Scalable log visualization for fault characterization in supercomputers. In *Proc. EGPGV*, pp. 91–100, 2018.
- [11] P. Hall and M. Hosseini-Nasab. Theory for high-order bounds in functional principal components analysis. In *Mathematical Proc. Cambridge Philosophical Society*, vol. 146, p. 225, 2009.
- [12] R. Higdon. Generalized additive models. In W. Dubitzky, O. Wolkenhauer, K.-H. Cho, and H. Yokota, eds., *Encyclopedia of Systems Biology*, pp. 814–815. Springer, 2013.
- [13] L. Horváth and P. Kokoszka. *Inference for Functional Data with Applications*. Springer, 2012.
- [14] R. J. Hyndman and M. Shahid Ullah. Robust forecasting of mortality and fertility rates: A functional data approach. *Computational Statistics & Data Analysis*, 51(10):4942–4956, 2007.
- [15] R. J. Hyndman and H. L. Shang. Rainbow plots, bagplots, and boxplots for functional data. *J. Computational and Graphical Statistics*, 19(1):29–45, 2010.
- [16] K. Karhunen. *Zur Spektraltheorie stochastischer Prozesse*. Annales Academiae scientiarum Fennicae. A.1, Mathematica-physica. 1946.
- [17] S. Katragadda, R. Gottumukkala, S. Venna, N. Lipari, S. Gaikwad, et al. VASStream: A visual analytics system for fast data streams. In *Proc. PEARC*, pp. 1–8, 2019.
- [18] S. P. Kesavan, T. Fujiwara, J. K. Li, C. Ross, M. Mubarak, et al. A visual analytics framework for reviewing streaming performance data. In *Proc. PacificVis*, pp. 206–215, 2020.
- [19] A. Kneip and K. J. Utikal. Inference for density families using functional principal component analysis. *J. the American Statistical Association*, 96(454):519–542, 2001.
- [20] M. Krstajic and D. A. Keim. Visualization of streaming data: Observing change and context in information visualization techniques. In *Proc. BigData*, pp. 41–47, 2013.
- [21] S. Kullback and R. A. Leibler. On information and sufficiency. *Annals of Mathematical Statistics*, 22(1):79–86, 1951.
- [22] S. Liu, J. Yin, X. Wang, W. Cui, K. Cao, and J. Pei. Online visual analytics of text streams. *IEEE Trans. on Visualization and Computer Graphics*, 22(11):2451–2466, 2016.
- [23] M. Loeve. *Fonctions al'éatoires a decomposition orthogonale exponentielle*, vol. 84 of *La Revue Scientifique*. 1946.
- [24] L. McInnes, J. Healy, and J. Melville. UMAP: Uniform manifold approximation and projection for dimension reduction. *arXiv:1802.03426*, 2018.
- [25] L. Millán-Roures, I. Epifanio, and V. Martínez. Detection of anomalies in water networks by functional data analysis. *Mathematical Problems in Engineering*, 2018:5129735, 2018.
- [26] H. Miyazaki, Y. Kusano, N. Shinjou, F. Shoji, M. Yokokawa, and T. Watanabe. Overview of the K computer system. *Fujitsu Scientific & Technical Journal*, 48(3):302–309, 2012.
- [27] T. T. Neves, R. M. Martins, D. B. Coimbra, K. Kucher, A. Kerren, et al. Xtreaming: An incremental multidimensional projection technique and its application to streaming data. *arXiv:2003.09017*, 2020.
- [28] B. H. Park, Y. Hui, S. Boehm, R. A. Ashraf, C. Layton, and C. Engelmann. A big data analytics framework for HPC log data: Three case studies using the titan supercomputer log. In *Proc. CLUSTER*, pp. 571–579, 2018.
- [29] B. H. Park, S. Hukerikar, R. Adamson, and C. Engelmann. Big data meets HPC log analytics: Scalable approach to understanding systems at extreme scale. In *Proc. CLUSTER*, pp. 758–765, 2017.
- [30] N. Pezzotti, B. P. Lelieveldt, L. van der Maaten, T. Höllt, E. Eisemann, and A. Vilanova. Approximated and user steerable tSNE for progressive visual analytics. *IEEE Trans. on Visualization and Computer Graphics*, 23(7):1739–1752, 2017.
- [31] J. O. Ramsay. Functional data analysis. In *Encyclopedia of Statistical Sciences*. American Cancer Society, 2006.
- [32] J. O. Ramsay and C. J. Dalzell. Some tools for functional data analysis. *J. Royal Stat. Society: Series B (Methodological)*, 53(3):539–561, 1991.
- [33] J. O. Ramsay and B. W. Silverman. *Functional Data Analysis*, p. 428. Springer-Verlag New York, 2005.
- [34] C. R. Rao. Some statistical methods for comparison of growth curves. *Biometrics*, 14(1):1–17, 1958.
- [35] D. A. Ross, J. Lim, R.-S. Lin, and M.-H. Yang. Incremental learning for robust visual tracking. *Int. J. Computer Vision*, 77(1-3):125–141, 2008.
- [36] H. Shang. A survey of functional principal component analysis. *Advances in Statistical Analysis*, 98:121–142, 2014.
- [37] F. Shilpika, B. Lusch, M. Emani, V. Vishwanath, M. E. Papka, and K.-L. Ma. MELA: A visual analytics tool for studying multifidelity hpc system logs. In *Proc. DAAC*, pp. 13–18, 2019.
- [38] Y. Tanahashi, C.-H. Hsueh, and K.-L. Ma. An efficient framework for generating storyline visualizations from streaming data. *IEEE Trans. on Visualization and Computer Graphics*, 21(6):730–742, 2015.
- [39] J. W. Tukey. Mathematics and the picturing of data. In *Proc. ICM*, vol. 2, pp. 523–531, 1975.
- [40] C. Turkay, E. Kaya, S. Balcisoy, and H. Hauser. Designing progressive and interactive analytics processes for high-dimensional data analysis. *IEEE Trans. on Visualization and Computer Graphics*, 23(1):131–140, 2017.
- [41] C. Turkay, N. Pezzotti, C. Binnig, H. Strobelt, B. Hammer, D. A. Keim, J.-D. Fekete, T. Palpanas, Y. Wang, and F. Rusu. Progressive data science: Potential and challenges. *arXiv:1812.08032*, 2018.
- [42] Y. Vardi and C.-H. Zhang. The multivariate L1-median and associated data depth. *PNAS*, 97(4):1423–1426, 2000.
- [43] R. Viviani, G. Grön, and M. Spitzer. Functional principal component analysis of fmri data. *Human Brain Mapping*, 24(2):109–129, 2005.
- [44] J.-L. Wang, J.-M. Chiou, and H.-G. Müller. Functional data analysis. *Annual Review of Statistics and Its Application*, 3(1):257–295, 2016.
- [45] Q. Wang, S. Zheng, A. Farahat, S. Serita, and C. Gupta. Remaining useful life estimation using functional data analysis. In *Proc. ICPHM*, pp. 1–8, 2019.
- [46] Y. Zuo, H. Cui, X. He, et al. On the Stahel-Donoho estimator and depth-weighted means of multivariate data. *The Annals of Statistics*, 32(1):167–188, 2004.